Fermi surface of Mo(112) and indirect interaction between adsorbed atoms

Ivan N. Yakovkin,[1,*] Keisuke Fukutani,[2] Hirokazu Hayashi,[3] Jian Jiang,[4] Taiki Horike,[3] Yorito Nagata,[3] Takafumi Habuchi,[3] Daisuke Hirayama,[3] Hideaki Iwasawa,[4] Kenya Shimada,[4] Ya. B. Losovyj,[2] and Peter A. Dowben[2]

[1]*Institute of Physics, National Academy of Sciences of Ukraine, Prospect Nauki 46, Kiev, UA 03028, Ukraine*

[2]*Department of Physics and Astronomy, Jorgensen Hall, P.O. Box 880299, University of Nebraska-Lincoln, Lincoln, Nebraska 68588-0299, USA*

[3]*Graduate School of Science, Hiroshima University, Higashi-Hiroshima 739-8526, Japan*

[4]*Hiroshima Synchrotron Radiation Center, Hiroshima University, 2-313 Kagamiyama, Higashi-Hiroshima 739-0046, Japan*

(Received 17 June 2012; published 4 September 2012)

A comprehensive examination of the Fermi surface of Mo(112) is presented. The Fermi surface contours for the Mo(112) surface, obtained by density functional theory calculations, agree well with the direct observations via angle-resolved photoemission spectroscopy and indicate the existence of flattened segments in the Fermi contours perpendicular to the direction of the atomic furrows. Both the calculation and the experiment indicate significant surface weight for these states. Such flattened Fermi contours at the surface can give rise to long-range charge density waves (CDW) and long-range indirect lateral interactions, especially in the case of adsorption of electropositive atoms. When mediated by the surface electrons, exhibiting flattened Fermi contours, the oscillatory potential of the indirect interaction between adsorbed atoms decays very slowly ($\sim 1/r$) in the direction along the furrows, which can explain the formation of long-period chain structures of electropositive adsorbates on the furrowed surface of Mo(112).

DOI: 10.1103/PhysRevB.86.125401 PACS number(s): 73.20.At, 63.20.kd, 73.61.At

I. INTRODUCTION

Some surfaces of molybdenum, in particular the (100) surface,[1–9] are well known for surface reconstructions driven by Peierls-like instability[10–12] that originates from charge density wave- (CDW-) driven transition coupling with the surface states at the Fermi level. The Peierls instability is induced by Fermi surface nesting (coincidence of the electronic states at the Fermi surface when shifted by the nesting wave vector $q = 2k_F$, where k_F is the Fermi wave vector) and is favored to occur in low-dimensional materials, anisotropic surfaces, and metals that have high densities of states at the Fermi level $N(E_F)$. For systems with a strong electron-phonon interaction, such properties can lead to surface reconstructions[9,13] with spatial periodicity that comes close to multiples of $2\pi/q$.

Not only does the CDW affect the surface structural stability, but as in the case of furrowed surfaces like Mo(112) as schematically illustrated in Fig. 1, many adsorbate layers adopt highly ordered long-period structures. In particular, at low coverages, most of alkali, alkaline earth, and rare-earth metals form linear chain adsorbate structures directed across the furrows (i.e., y direction in Fig. 1) on metallic surfaces, including Mo(112), resulting in commensurate $p(m \times 1)$ linear chain structures, where m is an integer.[14–45] While the period along this quasi-one-dimensional (linear) adsorbate chains formed on Mo(112) is dictated by the lattice constant of Mo(112) along the $\langle \bar{1}10 \rangle$ direction (4.45 Å), the distances between the chains in these structures correspond to m periods of the lattice constant of the furrows ($m \times$ 2.73 Å). The formation of these quasi-one-dimensional atomic chains oriented perpendicular to the furrows, in spite of the interfacial dipole-dipole repulsion $2\mu^2/r^3$ induced by the presence of adatoms at interatomic pair distance r,[24,46,47] implies the existence of an oscillatory indirect interaction, which results in the minima of the effective potential at interatomic distances adopted by the adatoms in the direction along the furrows.[24,39,41,43,48–53] Such indirect interaction stems from the Friedel oscillations[54] of electronic density of the substrate, formed for screening the charged adatoms, with the wavelength of π/k_F and related indirect lateral interaction potential given by $V_{ind}(r) \sim \cos(2k_F r + \delta)/r^n$.[24,39,41,43,48–55] The phase shift δ determines the position of the first minimum of the potential, while the "effectiveness" of the indirect interaction at large interatomic distances, with regard to the formation of long-period adlayer structures, critically depends on the asymptotic decay factor $1/r^n$. The asymptotic behavior of the indirect interaction strongly depends on the shape of Fermi surface.[24] For free electrons in a bulk metal, having a spherical Fermi surface, Lau and Kohn[49] suggested the $1/r^5$ behavior for the indirect interaction between charged impurity atoms. This means that in the case of a spherical Fermi surface, the lateral interactions between atoms on the surface decays rapidly and would be short range. With the rapid decay ($\sim 1/r^5$) of the adsorbate pair interactions, large-period adlayer structures at low coverage are unlikely to form because at large distances the dipole-dipole repulsion ($\sim 1/r^3$) dominates. To obtain long-period chain structures of adsorbed layers at low coverages, a persistent periodic potential is welcome. The screening in two-dimensional (2D) electron gas can provide much more efficient long-range interaction with a $1/r^2$ asymptotic decay.[24,47,49] Such 2D gas of free electrons can exist in Shockley surface states of close-packed noble metals.[56–61] For example, for Ag(111), the estimated value of the Fermi wave vector for the Shockley surface state is of 0.083 Å^{-1},[56] which corresponds to the wavelength of Friedel oscillations of ~38 Å, in agreement with the length of the observed CDW, as well as with the positions of the first minima of the potential of lateral interactions in adsorbed Co and Ce layers.[58,59] Yet, the more effective $1/r$ decay factor for the indirect interactions between adsorbate atoms that also provides the sufficient density of electrons required for formation of long-period

 ©2012 American Physical Society

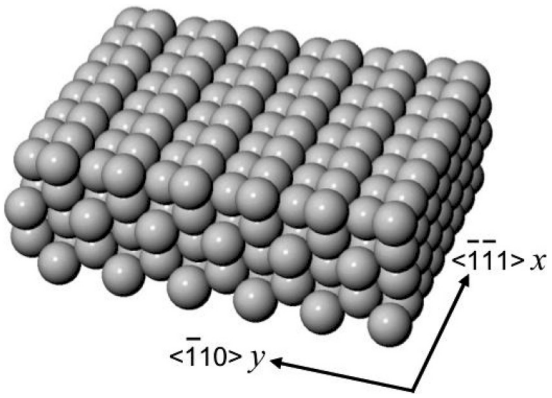

FIG. 1. The schematic representation of the Mo(112) surface. Crystallographic directions are labeled in relation to the Cartesian coordinate axes used in our discussion.

structures was predicted for quasi-one-dimensional systems having a flat segment in Fermi surface.[24,47,48]

It is intuitively clear that the strength of the interaction must depend on the number of electrons that take part in the Friedel oscillations. It is not just the density of states, but also the directions and regions in k space, where there is a significant density of states (DOS) at the Fermi level, matters (i.e., the k-resolved electronic structure is important). Thus, to better understand the rich physics of ordered long-period chain structures on Mo(112), the details of the Fermi surface must be understood in far greater detail than before. The Fermi wave vector of surface-weighted states (k_F) can be used to estimate the period of expected Friedel oscillations. Recently, there has been a reexamination of the complexities of the band structure of Mo(112).[62] In the present study, we extend this detailed examination of the band structure to explore the Fermi surface of Mo(112) and explore its implications on the ordering of quasi-one-dimensional adlayer structures on Mo(112).

II. EXPERIMENTAL DETAILS

The surface of the Mo(112) sample was cleaned by the standard method of repeated annealing (at $\sim$1400 °C) in an oxygen atmosphere with the oxygen partial pressure of $\sim 1 \times 10^{-6}$ torr, followed by cycles of annealing (at 1000–1300 °C) and flashing (at $\sim$1800 °C) similar to the procedures used elsewhere.[15–29,32–38,40,43,45,51–53,62] Low-energy electron diffraction (LEED) and Auger electron spectroscopy (AES) were used to verify the quality of the Mo(112) surface, including the periodic structural order. The amount of surface contamination, such as C and O, were evaluated to be below the detection limit of the AES. In addition, the presence of the surface-weighted state,[62] another signature of the clean surface, was confirmed in the spectrum of angle-resolved photoemission spectroscopy (ARPES), which can be seen in Fig. 2(a) as the state showing strong sensitivity to surface contamination (marked "Surface").

The high-resolution ARPES was performed at the linear undulator beamline (BL-1)[63] of Hiroshima Synchrotron Radiation Center (HiSOR) at Hiroshima University, Japan. The experiments were carried out using an angular (display) mode of the hemispherical electron analyzer (R4000, VG Scienta), with the acceptance angle of $\pm 15°$. The Fermi contour mapping was performed at the incident photon energy of $\hbar\omega = 50$ eV by rotating the sample in its surface plane by increments of 3°, using incident photon sources with both s- and p-polarization geometries (the vector potential of the incident light in the plane of the surface and 50° with respect to the surface normal, respectively). The band mapping along the $\bar{\Gamma} - \bar{\mathrm{X}}$ high-symmetry direction was also taken at several different photon energies with p-polarization geometry (with the vector potential lying 40° with respect to the surface normal). For both the Fermi contour mapping and the band mapping taken for a photon energy of 50 eV, the energy resolution was estimated to be $\sim$18 meV, and the angular resolution was $\leqslant 0.9°$, corresponding to a wave vector resolution of $\leqslant 0.054$ Å^{-1} at the Fermi level.

The temperature of the sample was maintained at $\sim$60 K by a constant flow of liquid helium. Since the sample was mounted on the sample holder with tungsten wires, there was inevitably a small tilt introduced to the sample alignment. The effect of such tilt on the band structure was nearly negligible and was accounted for during the data analysis.

III. THE THEORETICAL METHODOLOGY

The experimental band mapping of the Fermi surface of Mo(112) was compared to density functional theory (DFT) semirelativistic calculations in generalized gradient approximation.[64] The calculations were performed with the ABINIT[65] package using Troullier-Martins norm-conserving pseudopotentials.[66] The periodicity in the direction normal to the surface was maintained by adopting the repeat-slab model. The calculations were separately performed for the slabs built of 7, 9, and 11 layers of Mo(112) atomic planes. The vacuum gap was about 10 Å. The optimization of positions of atoms was performed until all forces became less than 0.05 eV/Å. The energy cutoff of 20 hartree provided the 0.001-hartree convergence of the total energy. Surface weights for every band and k point were estimated by the integration of the partial local electron density within the atomic spheres (with $r = 2.5$ Bohr).

Calculations of Fermi surfaces usually require k-point meshes of greater density than generally used for more "regular" DFT calculations that aim only to estimate the total energies for determination of the equilibrated structure or used to generate a calculated band structure and DOS. With a rough mesh of k points, some bands crossing E_F may be missed, which complicates the comparison with experimental Fermi surface. This is especially true here; the number of the bands increases dramatically for Mo(112), especially along the $\bar{\Gamma} - \bar{\mathrm{X}}$ direction, and some of the bands can cross the Fermi energy twice within the reduced surface Brillouin zone (SBZ) along the $\bar{\Gamma} - \bar{\mathrm{X}}$ direction.[61] Thus, while the 0.001-hartree convergence of the total energy was achieved with the $6 \times 4 \times 1$ grid of k points, the detailed Fermi surface of the Mo(112) could be obtained only with a $8 \times 5 \times 2$ grid and did not change significantly with further increases of the density of k points. The $16 \times 10 \times 2$ grid, giving 108 nonequivalent k points, was adopted for the calculations of the Mo(112) Fermi surface. The Fermi surfaces calculated

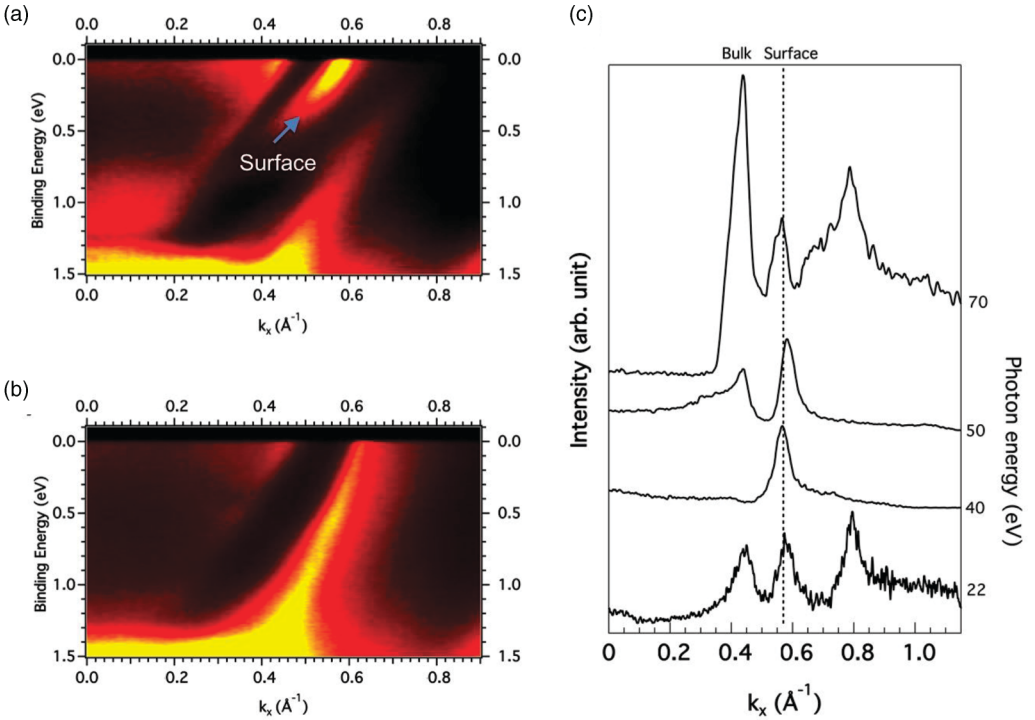

FIG. 2. (Color) The ARPES band mapping of Mo(112) along the $\bar{\Gamma} - \bar{X}$ direction in p-polarization geometry using 50-eV photon energy. The energy versus wave-number plot (a), taken shortly after the cleaning, clearly shows the surface-weighted band, labeled as "Surface," with $k_F = 0.59 \pm 0.02$ Å^{-1} that is estimated to have more than 78% charge localization within the first two layers.[62] In the energy versus wave-number plot (b), taken after adsorption of small amount of contamination (largely CO), the previously visible band "Surface" (a) is absent. The panel (c) shows the MDCs at the Fermi level taken with the incident photon energies of 22, 40, 50, and 70 eV and with p-polarization geometry.

from a 7- and 11-layer slab are illustrated in Fig. 3(a) and 3(b) respectively.

In the Monte Carlo simulations of the adsorbed layers within the lattice gas model, dynamical equilibration of a surface adlayer structure is achieved by moving randomly chosen particles to neighboring sites along the furrows.[39,41,50,67,68] The probability of each replacement (one "jump") of the particle is determined by the Boltzmann factor $\exp(-\Delta E/k_B T)$, or if the replacement leads to decrease of the total energy, that is, $\Delta E < 0$, the probability is taken to be unity. As a result of such an equilibration procedure (typically 10–20 jumps per particle are required), at low temperatures well-ordered structures of adlayers are formed, while at higher temperatures the adlayers become disordered. Relative intensity of the corresponding LEED images can then be evaluated in kinematical approximation, which gives the model $I(T)$ plot required for comparison with experiment. Consideration for the experimental parameters, in particular the typical coherence width for LEED, tends to favor a larger lattice, so we have chosen the size of the matrix to be about 100×100 Å^2, with periodic boundary conditions.

IV. THE FERMI SURFACE OF MO(112)

The band structure of Mo(112) along $\bar{\Gamma} - \bar{X}$ line is partly illustrated in the band mapping obtained from ARPES, shown in Figs. 2(a) and 2(b) (taken with 50-eV photon energy in p-polarization geometry). Figure 2(a) shows the short band diminishing toward higher binding energy with a Fermi level crossing at ~0.59 Å^{-1} labeled as "Surface." The recent band structure calculation shows that this band is strongly surface weighted and exhibits ~78% charge localization within the first two layers on Mo(112) with a large $d_{3z^2-r^2}$ contribution.[62] In fact, this band is seen to be very surface sensitive in the ARPES spectrum, as only a small amount of contamination (largely CO) destroys this surface-weighted state [see Fig. 2(b)]. In order to further verify the surface origin of this band, the momentum distribution curves (MDCs) at the Fermi level is plotted for four different photon energies in Fig. 2(c). From the photon energy dependence of the MDC spectra, it is evident that the k_F (i.e., the peak position of MDC) of the band labeled "Surface" only shows some photon energy dependence, mostly within the experimental error, and its intensity is persistent at least for the four different photon energies used here. Such insensitivity to the incident photon energy likely indicates some conservation of the two-dimensionality of this state (i.e., the surface state). The ARPES intensities of other two bands show the noticeable photon energy dependence and hence at least some bulk weight (in our recent study,[62] the band marked "bulk" in Fig. 2(c) is identified as a pure projected bulk state, and the unmarked band was suggested to be a surface resonance state). In this current study we are mainly concerned about the surface states and surface resonance states of Mo(112).

The Fermi surface of Mo(112), calculated for the 7-layer and 11-layer Mo(112) slabs, is shown in Figs. 3(a) and 3(b),

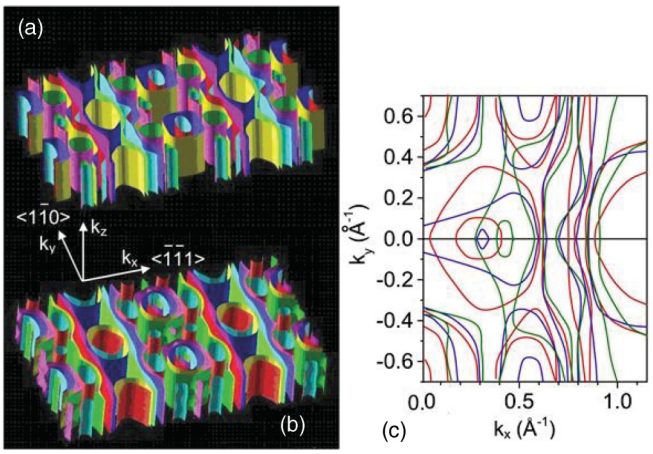

FIG. 3. (Color) The Fermi surface of Mo(112), calculated for the 7-layer (a) and 11-layer (b) Mo(112) slabs. The overlaid contour lines of the Fermi surface in the (112) plane calculated for the 7-layer (green), 9-layer (blue), and 11-layer (red) Mo(112) slabs in (c). Since the number of the bands crossing Fermi level depends on the thickness of the slab, the contours pertinent to particular thickness may be understood as representatives of the projection of a bulk Fermi surface, while those remaining essentially at the same position (so that they nearly coincide and thus do not depend on the thickness) are indicative for the Fermi contours with strong surface weights.

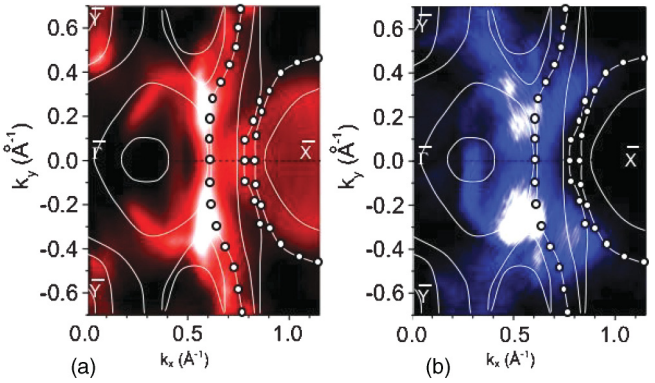

FIG. 4. (Color) The Fermi surface of Mo(112) obtained at the photon energy of 50 eV with (a) *p*- and (b) *s*-polarization geometry as described in detail in the experimental section. In both polarization geometries, the sample was rotated by the increment of 3° to obtain the presented image. The contours of the Fermi surface calculated for the 11-layer Mo(112) slab are overlaid. The calculated Fermi contour lines with dots indicate the Fermi contours with strong surface weight.

respectively. Since the number of the bands crossing the Fermi level depends on the thickness of the slab, the calculated Fermi surfaces do differ in some respects with the changes in the slab thickness. The calculated Fermi surfaces for the Mo(112) slabs of different thickness, nonetheless, show common features, which can be attributed to the segments of the Fermi surface pertinent to the Mo(112) surface. As the surface bands and surface resonance bands do not significantly depend on the thickness of the slab adopted in model calculations, only those bands that remain at nearly the same positions regardless of the number of layers are indeed characteristics of the surface.[62] The same is valid also for the contours of the Fermi surfaces in the (112) surface plane. Figure 3(c) shows the Fermi surface contours calculated with 7-layer (green), 9-layer (blue), and 11-layer (red) slab models. The Fermi contours remaining essentially at the same position (so that they nearly coincide and thus do not depend on the thickness) are indicative for the segments of Fermi surface with strong surface weights.

The maps of angle-resolved photoemission intensities at E_F for the SBZ of Mo(112) obtained for both *p*- and *s*-polarization geometries are shown in Figs. 4(a) and 4(b), respectively. The calculated contours of the Fermi surface using the 11-layer slab are overlaid, in which the circles (○) indicate the surface-weighted states. Comparison between the Fermi contour mapping taken with *p*- and *s*-polarization geometries enables us to use the dipole selection rules of photoemission to identify the symmetry properties of the electronic states along (or near) the high-symmetry directions. Due to the reflection symmetry of Mo(112) with respect to the xz plane, both the bulk and the surface electronic states along the $\bar{\Gamma}-\bar{X}$ line can be classified into either even or odd under the reflection about the xz plane. For the Fermi surface mapping taken with *p*-polarization geometry [Fig. 4(a)], since the surface-parallel component of the vector potential of the incident light lies along the x direction (when scanning along the $\bar{\Gamma}-\bar{X}$ line), the dipole selection rule reveals that the observed states (near the $\bar{\Gamma}-\bar{X}$ line) must be *even* under xz-plane reflection. On the other hand, with the *s*-polarization geometry [Fig. 4(b)], the similar argument can be made to conclude that the observed electronic states along the $\bar{\Gamma}-\bar{X}$ must be *odd* under xz-plane reflection.

It is important to note that, strictly speaking, the symmetry of Mo(112) is described by C_{1h} group (composed of the identity operation and the reflection about the $\bar{\Gamma}-\bar{X}$ axis, or xz plane). Therefore, we would not generally expect the electronic states along the $\bar{\Gamma}-\bar{Y}$ line to possess any nontrivial symmetry (i.e., the only symmetry operation for these states is identity operation). However, as can be seen in Fig. 4, the electronic states at ~0.45 Å^{-1} along $\bar{\Gamma}-\bar{Y}$ shows noticeable dependence on the incident light polarization (states clearly visible in *p*-polarization but almost invisible in *s*-polarization). In our experimental setup, this is the expected polarization dependence according to photoemission dipole selection rules when the state possesses the even symmetry with respect to the reflection about the $\bar{\Gamma}-\bar{Y}$ line. In fact, our calculations[62] suggest the dominant orbital characters of this band to be $d_{x^2-y^2}$, which is even with respect to the $\bar{\Gamma}-\bar{Y}$ line. Thus, although the strict C_2 invariance is absent for Mo(112) surface, the *near symmetry* is sufficient to produce the strong light polarization dependence in the photoemission experiment (within dipole approximation). For the above reason, the *near-even* symmetry (under reflection about $\bar{\Gamma}-\bar{Y}$) may be attributed to the states observed at k_y~0.45 Å^{-1}.

Of particular interest in the experimental Fermi surface mapping with the *p*-polarization geometry [Fig. 4(a)] is the nearly straight contour crossing the $\bar{\Gamma}-\bar{X}$ line at $k_x = 0.59 \pm 0.02$ Å^{-1}, close to the midway along this high-symmetry line. Our calculation and experiment indicate the significant surface weight for this contour throughout the SBZ, as signified by the circles (○) in Fig. 4. The strong intensity of this contour near the $\bar{\Gamma}-\bar{X}$ axis is absent in the map for *s*-polarization,

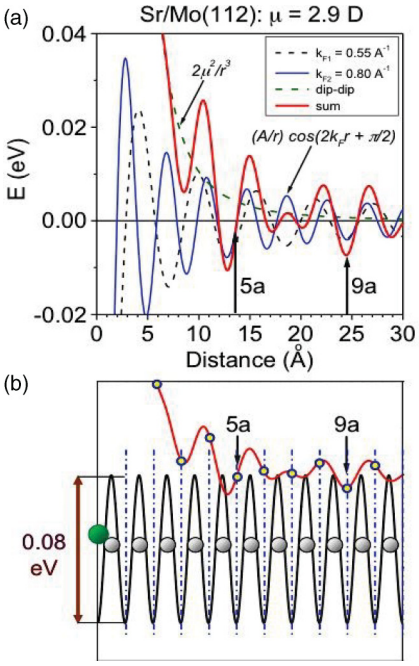

FIG. 5. (Color) The schematic of the effective potential for the lateral surface interaction along the furrows for Sr/Mo(112), resulting in widely spaced quasi-one-dimensional chains of Sr running perpendicular to the surface corrugation of Mo(112). (a) The potentials for Sr adatoms due to the surface-weighted states crossing E_F (or the sheets of the Fermi surface crossing the $\bar{\Gamma} - \bar{X}$ line) at $k_F = 0.58$ Å^{-1} and ~0.8 Å^{-1}, calculated using Eq. (1) with appropriate phase δ, are shown by a black dotted and blue solid curves, respectively. The effective potential, including the both surface-weighted states and the dipole-dipole interaction between Sr adatoms (green dashed line), is shown as a red/ solid curve. (b) Including considerations for the potential relief of the substrate, (the depth of the relief along Mo(112) furrows for Sr, calculated by Kiejna and Nieminen,[42] is 0.08 eV) the adatom separation of 9*a* becomes more favorable than that of 5*a* because of the *closer* match of the minima between the effective potential (red) and potential relief (black) of Mo(112).

which indicates that these states are of predominantly even symmetry with respect to the reflection about the $\bar{\Gamma} - \bar{X}$ line (and exactly even *on* $\bar{\Gamma} - \bar{X}$), in agreement with the previous identification.[62] The visible weak intensity smeared out along the $\bar{\Gamma} - \bar{X}$ line between 0.4 Å^{-1} and 0.65 Å^{-1} is likely attributed to the odd-symmetry bulk electron pockets identified in the earlier study.[62] The features of this flattened Fermi contour, for the Mo(112) surface, are in good agreement with the calculation, including the wave number k_x for this contour on the$\bar{\Gamma} - \bar{X}$ line, which is estimated to be 0.58 Å^{-1}.

The identified flattened segments perpendicular to the $\bar{\Gamma} - \bar{X}$ line (the direction of atomic furrows) provide a significant opportunity for Fermi surface nesting, which, in principle, can result in a number of phenomena such as induced surface reconstruction due to enhanced electron-phonon coupling, pronounced Kohn effect, and forming CDWs. In particular, surface reconstructions, induced by adsorption,[69–72] may well be aided by such nesting vectors.

V. THE INDIRECT INTERACTIONS AND ADLAYER CHAIN ORDERING AT LOW COVERAGES

The surface-weighted flat segments of the Fermi contour, as noted above, may well be essential for the quasi-one-dimensional behavior of the screening electrons at the Mo(112) surface. When mediated by these surface electrons in flattened segments of Fermi contour, the surface Friedel oscillations decay with the distance as $1/r$,[24,47,48] which provides an extremely efficient indirect interaction at large interatomic distances and can explain the formation of long-period chain structures for electropositive adsorbates on the furrowed transition metal surfaces.[24,39,41,43,48–53] Taking into account the dipole-dipole interaction, the potential of the lateral interaction between adsorbed particles in the direction along the furrows (i.e., normal to the flat sheets of the Fermi surface) is roughly[24,39,41,43,48–53]

$$V(r) = \frac{2\mu^2}{r^3} + \frac{A\cos(2k_F r + \delta)}{r}. \quad (1)$$

It is possible, in principle, to determine the A and δ from first principles, though the amplitude A and phase shift δ can also be chosen from the best fit to the observed adlayer periodicity. Because of the changes in the surface charge distribution arising from the adatoms adding or subtracting the charge to and from the surface, there is always the complication of changes in the Fermi contour changing with the addition of electropositive atoms at the surface; the addition of electropositive atoms at the surface will generally shift the Fermi-level crossings to larger wave vectors. However, for large interatomic distances between adsorbate chains, the accuracy of calculations within the slab model is often also limited because of greatly increased computational time for larger unit cells containing many transition metal atoms. It is often desirable to simply choose the phase shift to fit one of the minima of the potential to the favorable interatomic distance observed in the experiment. The dipole moment μ of adsorbed electropositive atoms can be derived from the rate of the decrease of work function through the Helmholtz equation.

For Mo(112), the spatial period of oscillations of the potential for the electropositive adlayers along the atomic furrow (i.e., x direction in Fig. 1) seems to fall between four and five periods of the substrate lattice constant ($a = 2.73$ Å). For example, at low coverages, Li and Mg on Mo(112) form the $p(4 \times 1)$ structure, while Sr and Ba form the $p(5 \times 1)$ structure.[15–39] For Sr, another minimum of the potential of the indirect interaction along the furrows has been found at nine lattice constants ($9a = 24.6$ Å).[57] The $p(9 \times 1)$ structure starts to form at coverages well below 1/9 of a monolayer, which indicates the growth of islands of $p(9 \times 1)$ structure, and with increasing coverage, transforms to the $p(5 \times 1)$ structure, whereas intermediate structures [like $p(8 \times 1)$, $p(7 \times 1)$, and $p(6 \times 1)$] are not observed.[17,18,39,57] Hence, the minimum of the potential for Sr adlayer at 9*a* must be deeper than at 5*a*—this is necessary for the formation of the $p(9 \times 1)$ rather than the $p(5 \times 1)$ structure at low coverages.

The Fermi wave vector determined both from the ARPES experiment (0.59 ± 0.02 Å^{-1}), and the calculations (0.58 Å^{-1}) for the prominent surface-weighted band are in agreement and roughly correspond to the wavelength of the surface CDW of

approximately 5.4 Å. The effective potential for Sr adatoms due to this surface-weighted state is thus calculated using Eq. (1) with the appropriate phase δ and shown as black dotted curves in Fig. 5(a). In this graph, the minima at $5a$ and $9a$ can be identified, which are in fact expected. On the other hand, another minimum at $\sim 7a$ should also be identified, which apparently gives rise to the formation of a $p(7 \times 1)$ structure for intermediate Sr coverage, not observed in the experiments. However, the possible contributions from all the surface-weighted bands to the indirect effective potential should be considered before drawing the conclusion. This means that the other surface-weighted band that participates in the surface screening, with a different Friedel oscillation period, must be taken into account, and with this inclusion, we find the collective sum canceling out the minimum at $7a$ expected in the most naïve picture, as will be discussed below. The addition of the band crossing E_F (or the sheet of the Fermi surface crossing the $\bar{\Gamma} - \bar{X}$ line) at ~ 0.8 Å^{-1} should provide a more complete picture and the proper spatial dependence of the potential. The potential, including both the surface-weighted states with $k_F = 0.58$ and 0.80 Å^{-1} and the dipole-dipole interaction between Sr adatoms, is shown as a red solid curve in Fig. 5(a). Note that the potential minimum at $7a$ has disappeared.

The adatom separation of $9a$ becomes more favorable than that of $5a$ because of the *closer* match of the minima between the effective potential (red) and potential relief (black) of Mo(112) when there is due consideration for the potential relief of the substrate, as illustrated by Fig. 5(b). This is based on a depth of the potential relief for the diffusion of Sr adatoms along Mo(112) furrows as calculated by Kiejna and Nieminen,[42] of the order 0.08 eV. Therefore, at Sr coverages less than 1/9 of a monolayer, the formation of the $p(9 \times 1)$ structure should still be expected, while the $p(5 \times 1)$ structure will start to form for coverages above 1/9 monolayer. It should be noted also that the preference of the $p(9 \times 1)$ structure at low coverages likely indicates that the minimum of the net lateral potential for the $9a$ distance is deeper than for $5a$, which can be obtained only with the sufficiently slow asymptotic decay of the potential of indirect interaction in Eq. (1) for Mo(112).

Obviously, the suggested model potential, presented in Fig. 5, provides only a qualitative (or semiquantitative) description of the lateral interactions between Sr adatoms. The potential has been generated using Eq. (1) assuming, somewhat arbitrarily, the same amplitudes A of Friedel oscillations for screening electrons in different sheets of Fermi surface and which were chosen to yield reasonable values of the lateral interactions. It should be noted also that the depth of the various minima of the potential found here are in agreement with results of DFT calculations by Kiejna and Nieminen.[42] It perhaps should be noted that these variations on the contour of this corrugated surface (the minima) are about an order of magnitude smaller than the depth of the potential relief along the furrows [see Fig. 5(b)]. The fact that these minima of the potential energy contour, due to surface electrons, are quite shallow means that there are some limitations to the accuracy of these model calculations. With these deficiencies in mind, the model does demonstrate that the flat segments of the Fermi surface can explain (at least, in principle) the formation of the long-period chain structures observed at low coverages of Sr on Mo(112).[17,18,39]

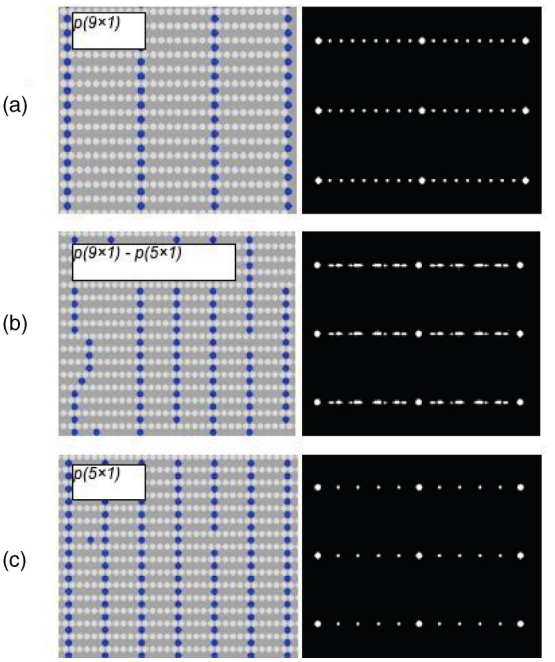

FIG. 6. (Color online) Snapshots of adsorbate ordering, abstracted from a sequence of Monte Carlo simulations for characteristic Sr coverages on Mo(112), and these are provided together with the related model LEED patterns, seen to be in agreement with experiment.[18] The $p(9 \times 1)$ structure is formed at coverages below and equal to 1/9 monolayer (a). With increasing coverage, the phase transition from the $p(9 \times 1)$ to $p(5 \times 1)$ structure reveals itself in characteristic coupling of LEED reflections (b). The formation of the p(5×1) structure is completed at the coverage of 1/5 monolayer (c).

With an estimate of the dependence of the lateral interaction on the distance between adatoms, the formation of chain structures can be visualized through Monte Carlo simulations, using the standard Metropolis technique within the lattice-gas model. In Fig. 6, the snapshots obtained in the course of the simulations with parameters of the lateral interaction [denoted by circles in Fig. 5(b)], are shown for characteristic Sr coverages together with related model LEED patterns. The phase transition from the $p(9 \times 1)$ structure, forming at a adlayer coverage of 1/9 monolayer to the $p(5 \times 1)$ structure as the coverage increases, reveals itself in the characteristic coupling of the LEED reflections, in perfect agreement with experiment.[18]

The surface CDW, in principle, can be visualized by scanning transmission microscopy (STM), as has been demonstrated in number of studies performed on close-packed noble and some transition metal surfaces. The Mo(112) surface, however, is a difficult surface to image the surface CDW because of the complexity in preparing a clean surface with the quality sufficient for obtaining good STM images at the necessary low bias.[73] Alkali and alkaline earth metals are also notoriously difficult to image in STM because of the strong hybridization of the frontier s-orbital with the substrate. It is useful, nonetheless, to predict how the CDW will appear in STM, and this can be simulated using the Tersoff-Hamann method.[74] The model STM picture is shown in Fig. 7 for the

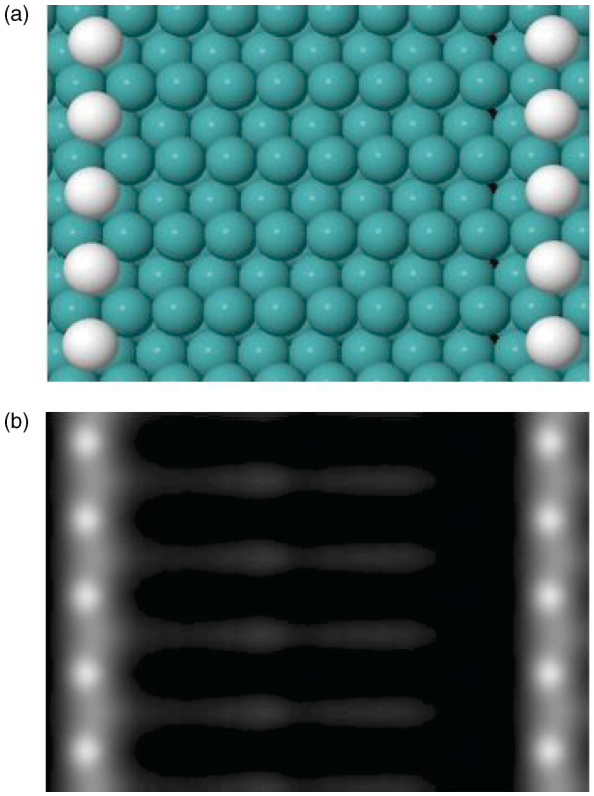

FIG. 7. (Color online) The $p(9 \times 1)$ Sr structure on Mo(112) surface (a) is compared to the model scanning tunneling (STM) image (b). The induced CDW should be revealed in the modulation of the brightness of the image of Mo atoms of the rows, i.e., modulation of the intensity along the direction of the substrate corrugation.

case of the $p(9 \times 1)$ Sr adlayer structure on Mo(112). It is seen that the brightness of the images of the atoms of the surface Mo(112) substrate rows is modulated by the CDW with the period of about $2a$, consistent with the $k_F = 0.58$ Å^{-1} along the $\bar{\Gamma} - \bar{X}$ line by the flattened segment of Fermi contour.

VI. CONCLUSION

The Fermi surface contour of Mo(112) are calculated and are mapped in angle-resolved photoemission. Fermi surface contour images in ARPES are seen to exhibit different features with p- and s-polarization geometries. These differences are attributed to the different symmetries of the surface-weighted bands crossing the Fermi level and consistent with prior band mappings.[24,62,69,75–77] The most prominent feature of the Mo(112) Fermi contour, identified both in the ARPES experiment and in our calculation, is the existence of flattened contours perpendicular to the $\langle \bar{1}\bar{1}1 \rangle$ direction [i.e., perpendicular to the surface furrows of Mo(112) substrate]. The electrons associated with the flattened contours of the Fermi surface are expected to give rise to well pronounced surface CDWs, especially in the case of adsorption of electropositive atoms. The related oscillatory potential of the indirect interaction between adsorbed atoms decays as $1/r$ in the direction along $\langle \bar{1}\bar{1}1 \rangle$ direction, which may explain the formation of long-period chain structures of electropositive adsorbates on Mo(112) surface.

ACKNOWLEDGMENTS

This work was partially supported by the IMI Program of the National Science Foundation under Award No. DMR 0843934 and the UNL NSF "QSPINS" MRSEC (DMR-0820521). The authors acknowledge Koji Miyamoto and Eike F. Schwier at the HiSOR for a number of valuable discussions. The synchrotron radiation measurements have been done with the approval of HSRC (Proposals No. 10-B-32 and No. 12-A-2). We thank the N-BARD of Hiroshima University for supplying liquid helium.

*Corresponding author: yakov@iop.kiev.ua

[1] T. E. Felter, R. A. Barker, and P. J. Estrup, Phys. Rev. Lett. **38**, 1138 (1977).
[2] M. K. Debe and D. A. King, Phys, Rev. Lett. **39**, 708 (1977).
[3] J. W. Chung, K. S. Shin, D. H. Baek, C. Y. Kim, H. W. Kim, S. K. Lee, C. Y. Park, T. Kinoshita, M. Watanabe, A. Kakizaki, and T. Ishii, Phys. Rev. Lett. **69**, 2228 (1992).
[4] K. E. Smith and S. D. Kevan, Phys. Rev. B **43**, 3986 (1991).
[5] X. W. Wang, C. T. Chan, K. M. Ho, and W. Weber, Phys. Rev. Lett. **60**, 2066 (1988).
[6] I. Terakura, K. Terakura, and N. Hamada, Surf. Sci. **103**, 103 (1981).
[7] E. Hulpke and D. M. Smilgies, Phys. Rev. B **40**, 1338 (1989).
[8] J. E. Inglesfield, J. Phys. C **11**, L69 (1978).
[9] J. E. Inglesfield, J. Phys. C **12**, 149 (1979).
[10] R. E. Peierls, *Quantum Theory of Solids* (Oxford University Press, Oxford, 1955).
[11] E. Tosatti, Solid State Commun. **25**, 637 (1978).
[12] J. C. Campuzano, D. A. King, C. Somerton, and J. E. Inglesfield, Phys. Rev. Lett. **45**, 1649 (1980).
[13] M. D. Johannes and I. I. Mazin, Phys. Rev. B **77**, 165135 (2008).
[14] J. M. Chen and C. A. Papageorgopoulos, Surf. Sci. **21**, 377 (1970).
[15] M. S. Gupalo, V. K. Medvedev, B. M. Palyukh, and T. P. Smereka, Fiz. Tverd. Tela **34**, 368 (1973).
[16] V. K. Medvedev, A. G. Naumovets, and T. P. Smereka, Surf. Sci. **34**, 368 (1973).
[17] V. K. Medvedev and I. N. Yakovkin, Fiz. Tverd. Tela (Leningrad) **20**, 928 (1978).
[18] V. K. Medvedev and I. N. Yakovkin, Fiz. Tverd. Tela (Leningrad) **21**, 313 (1979).
[19] F. M. Honchar, V. K. Medvedev, T. P. Smereka, Ya. B. Losovyj, and H. V. Babkin, Sov. Phys. Solid State **21**, 568 (1979).
[20] V. K. Medvedev and I. N. Yakovkin, Fiz. Tverd. Tela (Leningrad) **23**, 669 (1981).
[21] I. F. Lyuksyutov, V. K. Medvedev, and I. N. Yakovkin, Sov. Phys. JETP **81**, 2452 (1981).
[22] V. K. Medvedev and I. N. Yakovkin, Poverkhnost **5**, 112 (1982).
[23] F. M. Honchar, V. K. Medvedev, T. P. Smereka, Ya. B. Losovyj and H. V. Babkin, Fiz. Tverd. Tela (Leningrad) **29**, 2833 (1987).
[24] O. M. Braun and V. K. Medvedev, Sov. Phys. Usp. **32**, 328 (1989).

[25]I. F. Lyuksyutov, A. G. Naumovets, and V. Pokrovsky, *Two-Dimensional Crystals* (Academic Press, Boston, 1992).
[26]G. A. Katrich, V. V. Klimov, and I. N. Yakovkin, Ukr. J. Phys. **37**, 429 (1992).
[27]G. A. Katrich, V. V. Klimov, and I. N. Yakovkin, J. Electron Spectrosc. Relat. Phenom. **68**, 369 (1994).
[28]J. Zhang, D. N. Mcllroy, and P. A. Dowben, Phys. Rev. B **49**, 13780 (1994).
[29]J. Zhang, D. N. Mcllroy, and P. A. Dowben, Phys. Rev. B **52**, 11380 (1995).
[30]Ya. B. Losovyj, Vacuum **48**, 195 (1997).
[31]I. N. Yakovkin, G. A. Katrich, A. T. Loburets, Yu. S. Vedula, and A. G. Naumovets, Prog. Surf. Sci. **59**, 355 (1998).
[32]Ya. B. Losovyj, Vacuum **54**, 19 (1999).
[33]Ya. B. Losovyj and N. T. Dubyk, Vacuum **54**, 25 (1999).
[34]A. Fedorus, D. Kolthoff, V. Koval, I. Lyuksyutov, A. Naumovets, and H. Pfnuer, Phys. Rev. B **62**, 2852 (2000).
[35]A. Fedorus, G. Godzik, V. Koval, A. Naumovets, and H. Pfnur, Surf. Sci. **460**, 229 (2000).
[36]D. Kolthoff and H. Pfnur, Surf. Sci. **457**, 134 (2000).
[37]D. Kolthoff and H. Pfnur, Surf. Sci. **459**, 265 (2000).
[38]A. G. Fedorus, V. P. Koval, A. G. Naumovets, and H. Pfnuer, Fiz. Nizk. Temp. **27**, 68 (2001).
[39]I. N. Yakovkin, J. Nanosci. Nanotechnol. **1**, 357 (2001).
[40]G. Godzik, T. Block, and H. Pfnur, Phys. Rev. B **67**, 125424 (2003).
[41]I. N. Yakovkin, Surf. Sci. **559**, 29 (2004).
[42]A. Kiejna and R. M. Nieminen, Phys. Rev. B **69**, 235424 (2004).
[43]Ya. B. Losovyj, I. N. Yakovkin, H. K. Jeong, D. Wisbey, and P. A. Dowben, J. Phys.: Condens. Matter **16**, 4711 (2004).
[44]I. N. Yakovkin, Appl. Surf. Sci. **252**, 6127 (2006).
[45]M. Kuchowicz and J. Kolaczkiewicz, Surf. Sci. **603**, 1018 (2009).
[46]T. T. Tsong, Phys. Rev. B **6**, 417 (1972).
[47]T. L. Einstein, Crit. Rev. Solid State Mater. Sci. **7**, 261 (1978).
[48]Cz. Oleksy and J. Lorenc, Phys. Rev. B **54**, 5955 (1996).
[49]K. H. Lau and W. Kohn, Surf. Sci. **75**, 69 (1978).
[50]I. N. Yakovkin, Surf. Sci. **282**, 195 (1993).
[51]R. Szukiewicz, J. Kołaczkiewicz, and I. N. Yakovkin, Surf. Sci. **602**, 2610 (2008).
[52]M. Wiejak, M. Jankowski, I. N. Yakovkin, and J. Kołaczkiewicz, Appl. Surf. Sci. **256**, 4834. (2010).
[53]J. Sliwinski, M. Wiejak, Sz. Klein, J. Kolaczkiewicz, and I. N. Yakovkin, Surf. Sci. **606**, 21 (2012).
[54]J. Friedel, Philos. Mag. **43**, 153 (1952).
[55]T. B. Grimley, Proc. Phys. Soc. London **90**, 751 (1967).
[56]O. Jeandupeux, L. Bürgi, A. Hirstein, H. Brune, and K. Kern, Phys. Rev. B **59**, 15926 (1999).
[57]P. Hyldgaard and M. Persson, J. Phys.: Condens. Matter **12**, L13 (2000).
[58]J. Repp, F. Moresco, G. Meyer, K.-H. Rieder, P. Hyldgaard, and M. Persson, Phys. Rev. Lett. **85**, 2981 (2000).
[59]N. Knorr, H. Brune, M. Epple, A. Hirstein, M. A. Schneider, and K. Kern, Phys. Rev. B **65**, 115420 (2002).
[60]M. Kulawik, H.-P. Rust, M. Heyde, N. Nilius, B.A. Mantooth, P. S. Weiss, and H.-J. Freund, Surf. Sci. **590**, L253 (2005).
[61]N. N. Negulyaev, V. S. Stepanyuk, W. Hergert, H. Fangohr, and P. Bruno, Surf. Sci. **600**, 58 (2006).
[62]K. Fukutani, H. Hayashi, I. N. Yakovkin, T. R. Paudel, T. Habuchi, D. Hirayama, J. Jiang, H. Iwasawa, K. Shimada, N. Wu, E. Y. Tsymbal,Ya. B. Losovyj, and P. A. Dowben, Phys. Rev. B **85**, 155435 (2012).
[63]K. Shimada, M. Arita, Y. Takeda, H. Fujino, K. Kobayashi, T. Narimura, H. Namatame, and M. Taniguchi, Surf. Rev. Lett. **9**, 529 (2002).
[64]J. P. Perdew, K. Burke, and M. Ernzerhof, Phys. Rev. Lett. **77**, 3865 (1996).
[65]X. Gonze, J.-M. Beuken, R. Caracas, F. Detraux, M. Fuchs, G.-M. Rignanese, L. Sindic, M. Verstraete, G. Zerah, F. Jollet, M. Torrent, A. Roy, M. Mikami, Ph. Ghosez, J.-Y. Raty, and D. C. Allan, Comput. Mater. Sci. **25**, 478 (2002).
[66]N. Troullier and J. L. Martins, Phys. Rev. B **43**, 1993 (1991).
[67]N. Metropolis, A. W. Rosenbluth, M. N. Rosenbluth, A. H. Teller, and E. Teller, J. Chem. Phys. **21**, 1087 (1953).
[68]T. T. Tsong, Surf. Sci. **122**, 99 (1982).
[69]T. McAvoy, J. Zhang, C. Waldfried, D. N. McIlroy, P.A. Dowben, O. Zeybek, T. Bertrams, and S. D. Barrett, Eur. Phys. J. B **14**, 747 (2000).
[70]D. Kolthoff, H. Pfnür, A. G. Fedorus, V. Koval, and A. G. Naumovets, Surf. Sci. **439**, 224 (1999).
[71]T. Schroeder, J. B. Giorgi, A. Hammoudeh, N. Magg, M. Bäumer, and H.-J. Freund, Phys. Rev. B **65**, 115411 (2002).
[72]T. Schroeder, J. Aegenhagen, N. Magg, B. Immaraporn, and H.-J. Freund, Surf. Sci. **552**, 85 (2004).
[73]I. N. Yakovkin, M. Kuchowicz, R. Szukiewicz, and J. Kołaczkiewicz, Surf. Sci. Lett. **600**, L240 (2006).
[74]J. Tersoff and D. R. Hamann, Phys. Rev. Lett. **50**, 1998 (1983).
[75]I. N. Yakovkin, J. Zhang, and P. A. Dowben, Phys. Rev. B **63**, 115408 (2001).
[76]H.-K. Jeong, T. Komesu, I. N. Yakovkin, and P. A. Dowben, Surf. Sci. Lett. **494**, L773 (2001).
[77]N. Wu, Ya. B. Losovyj, Z. Yu, R. F. Sabirianov, W. N. Mei, N. Lozova, J. A. Colón Santana, and P. A. Dowben, J. Phys.: Condens. Matter **21**, 474222 (2009).